CHAPTER 5

SHAPE CONTROLLED SYNTHESIS OF Au NANOPARTICLES

This chapter explores the growth morphology of synthesized gold nanoparticles through seed based approach. The detailed structural characterization of the Au nanoparticles is being carried through TEM. The special crystallographic features of various types of morphologies observed has been discussed. The influence of shape on the LSPR behavior is also the subject of this chapter. After introducing various structural modifications reported in Au NPs, experimental methods have been described. The results and discussion is given in a separate section. Conclusions is presented at the end of this chapter.

5.1 Introduction

Phase transformation in elemental gold at a length scale less than 100 nanometers has received considerable attention owing to observation of newer phases hitherto unknown in microscopic systems. Such studies got fresh impetus after identifying parameters for precise control of synthesis protocol in wet chemical methods [199–206]. The structural and microstructural modifications are important for desired properties. The face centered cubic gold has been reported to form tetragonal, orthorhombic, and hexagonal phases depending on size and shape of gold crystallites [52, 53]. All these phases have distinct structural characteristics and depict different face forms apart from usual pentagonal twins observed in gold particles both in native and synthetic states [52, 53]. Au NPs are

finding uses in many of the important fields ranging from theranaustics to plasmonics [125, 207–211]. There are two relevant issues to be addressed for these applications, viz., stability of nanoparticles and control of their shapes. Plasmon behaviors are dictated by shape and size [116]. The required characteristics related to these can be attained through proper design of synthesis protocol. Seed based growth of nanoparticles is ideally suited for this purpose [199, 205, 212, 213]. The objectives of this chapter is to demonstrate this aspect. Apart from aforesaid issues pertaining to applications, identifying stimulus of phase transformations is scientifically challenging to understand microstructural features and structural changes. There are two technical issues that are to be delineated in this context. They refer to local structural transformation and shape change during the process of growth. Both could either be occurring concurrently or independently. It seems that irrespective of these two possibilities, agencies responsible for the structural and microstructural transformations seem to be different. Subtle change in the stacking sequence in a single component system can be attributed to nature of the stacking faults [203, 214, 215]. These are essentially growth fault. The shape of the particles is closely related to underlying symmetries of the crystals. It may be recalled that cubic close packed (CCP) gold has three rotational symmetries -2-, 3-, and 4-folds. The pentagonal or decahedral morphologies of gold particles have their origin in the nature of nuclei during nucleation process. It is easier to interpret and comprehend growth morphologies if one assumes shape of the seed/nuclei to possess higher point group symmetry. This should belong to a supergroup of cubic point group. All other shapes under different conditions of growth can arise as a consequence of symmetry breaking. If the seed is spherical then

there is a possibility of spherical particle morphology under condition of isotropic growth otherwise facetted growth morphology will result. Pentagonal, decahedral, triangular, hexagonal, rod like morphologies or any other shape being observed may all be due to anisotropic growth condition prevailing at the interface between the transformed aggregate regions and atoms that are willing to be a part of such a region [216, 217]. It may be realized that if growth rate is fast, high symmetry directions will be the slowest direction for growth and thus will control the shape of resulting particles. The size of various faces of the particles will be dictated by low symmetry direction. The shape, therefore, will be controlled by high symmetry direction of nuclei and size will be governed by its low symmetry axis. It will be through induction that one may see these factors being operative in the present investigation. All these are being arrived at based on transmission electron microscopic observations. The two aspects of such an observation refer to shape of the particles and their contrast on one hand and subtle diffraction features around the Braggs peak on the other. It has been mentioned in literature that under kinematical conditions, the symmetry of particle shape gets reflected in the fine structure around the Braggs peaks [218]. These fine structures arise owing to shape transform of the particle and the limit on size of observing them is below 100 nm. This effect is expected to arise around all the Braggs peaks. For nanoparticles research, this aspect has already been deliberated in the literature [218].

5.2 Experimental details

5.2.1 Preparation of Au seed

Twenty-two μL of 115.6 mM aqueous $HAuCl_4.3H_2O$ solution was mixed in a solution consisting of 68 mg PVP, 45 mL DMF, and 2.5 mL deionized water. This solution was agitated magnetically for about 30 min. In the above solution freshly prepared 2.5 mL 10 mM $NaBH_4$ was added and stirred for 2 h. A light pink color Au suspension obtained. This suspension was left for 24 h to completely decompose $NaBH_4$. Such a suspension will be referred to as seed solution subsequently.

5.2.2 Synthesis of faceted Au nanoparticles

7.5 mL 10 mM PVP solution in DMF and 420 µL 115.6 mM aqueous $HAuCl_4.3H_2O$ solution were mixed. This will be referred to as growth solution hereafter. Such a solution was ultrasonicated with a probe sonicator (60W was utilized out of 500 W available as maximum power) till vibrant yellow color disappeared. In this, 700 µL of Au seed solution was added and ultrasonicated for 2 h. Samples were collected after 10 min, 20 min, 30 min, 1 h, and 2 h after addition of seed solution. The samples were washed to remove impurities by centrifugation and ultrasonication with acetone and methanol mixture for at least three times. The powder thus obtained was dispersed in methanol and a drop was placed on carbon-coated Cu grid for morphological and structural characterization with transmission electron microscope (FEI Tecnai G^2 T20 operating at 200 kV). The surface plasmonic response of the Au nanoparticles was assessed with UV-Vis-NIR spectrometer.

5.3 Results and discussion

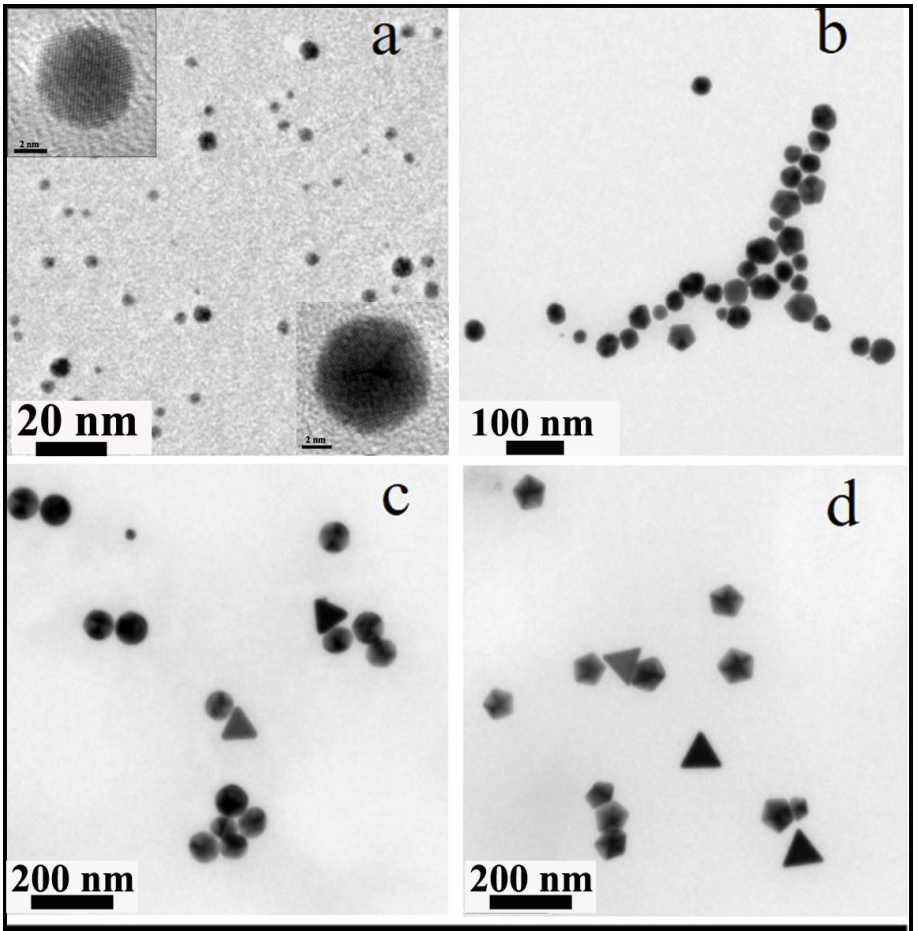

Shapes	10 min	20 min	30 min	1 hr	2 hr
Pentagons	25	12	83	84	79
Triangles	0	17	13	13	19
Hexagon	31	4	4	3	2
Others	44	67	-	-	-

FIGURE 5.1: Temporal evolution of morphology (a) seed, (b) 10 min, (c) 20 min and (d) 30 min grown samples. Inset in (a) shows seed morphology at higher magnification. Population statistics of shapes is given in table.

5.3.1 Morphological and structural study

Temporal evolution of faceted nanocrystals growth has been studied with the help of TEM and these are shown in Figure 5.1. Population statistics of various shapes is also summarized in the bottom of this Figure.

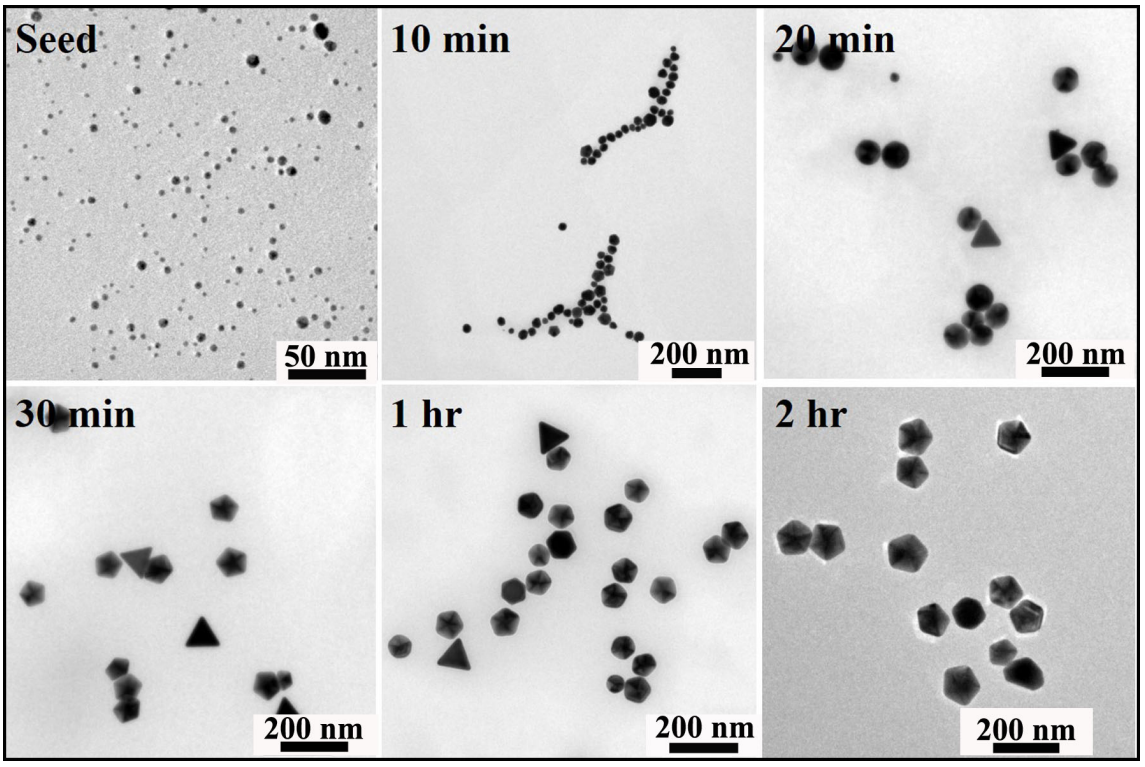

FIGURE 5.2: Morphology evolution of Au NPs with respect to time upto 2 h.

Aliquots were taken at time interval of 0 min (seeds), 10 min, 20 min, 30 min, 1 h (cf. Fig. 5.2) and 2 h (Fig. 5.2) and their morphologies were observed in TEM. The seeds (0 min) show dimension of NPs of $\sim$ 2-10 nm. The two predominant morphologies when observed under HRTEM has been shown as insets. They refer to nearly spherical (top left inset in Figure 5.1 a) and faceted pentagonal seeds (bottom right inset in Figure 5.1 (a)). These observations are commensurate with respect to a supergroup of these seeds (section 5.1). After 10 minutes of growth average particle sizes show polydispersity based

on morphology. Around 25% of seeds were observed to be pentagons, 31% of hexagons, and 44% of other irregular shapes. Their average lateral dimensions are $\sim$ 31 nm, 27 nm, and 32 nm, respectively. Whereas after 20 minutes, pentagonal shapes have been reduced to 12%. A new triangular shape has been evolved with a population of $\sim$ 17%, hexagonal shapes has been reduced to only 4% whereas a very large population of $\sim$ 67% were found to be pseudospherical. When closely inspected under HRTEM they were found to be prominently faceted and having pentatwins in most of them. Their lateral dimensions are $\sim$ 40, 77, 37 and 73 nm, respectively. After 30 minutes, the population of sharp pentagons has been increased to $\sim$ 83% whereas population of triangular and hexagonal particles are $\sim$ 13% and $\sim$ 4% which is essentially constant within the statistical error limit of our sampling size of $\sim$ 200 particles. The pseudospherical particles which were observed in the 20 minute aliquots were not observed. The same trend of the 30 minute aliquots were continued for 1 h and 2 h periods of growth. The nominal population of 2 h grown sample is 79%, 19% and 2% for pentagons, triangular and hexagons, respectively. This statistical population distribution is shown in the form of Table in Figure 5.1. Foregoing discussion demonstrates fast growth along 2-fold directions. The overall shape of the nanoparticles is due to high symmetric direction possessing relatively lower growth rate. For triangular particle, this refers to three-fold direction whereas for the pentagonal one, this relate to five-fold direction.

It is observed that $NaBH_4$ reduction of $HAuCl_4$ in DMF gives rise to ultra-small faceted Au NPs which under ultrasonic irradiation and in presence of Au (I) complex gradually grows following the facets already present in the seed [202, 210]. In 20

minute grown sample, clear evolution of pentagons, triangular, hexagonal and pseudo-spherical shapes underlines the fastest growth in 2-fold direction and slow growth in 3-fold direction which is evident from the observation that all the shapes are bounded by 3-fold facets. In 30 minutes sample disappearance of this pseudospherical shapes and increase in the population of pentagonal shapes allow us to infer that (i) experimental conditions favor pentatwinned growth which is also evident from the presence of pentatwins in pseudospherical Au NPs and (ii) the almost fixed ratio of triangular and hexagonal particles

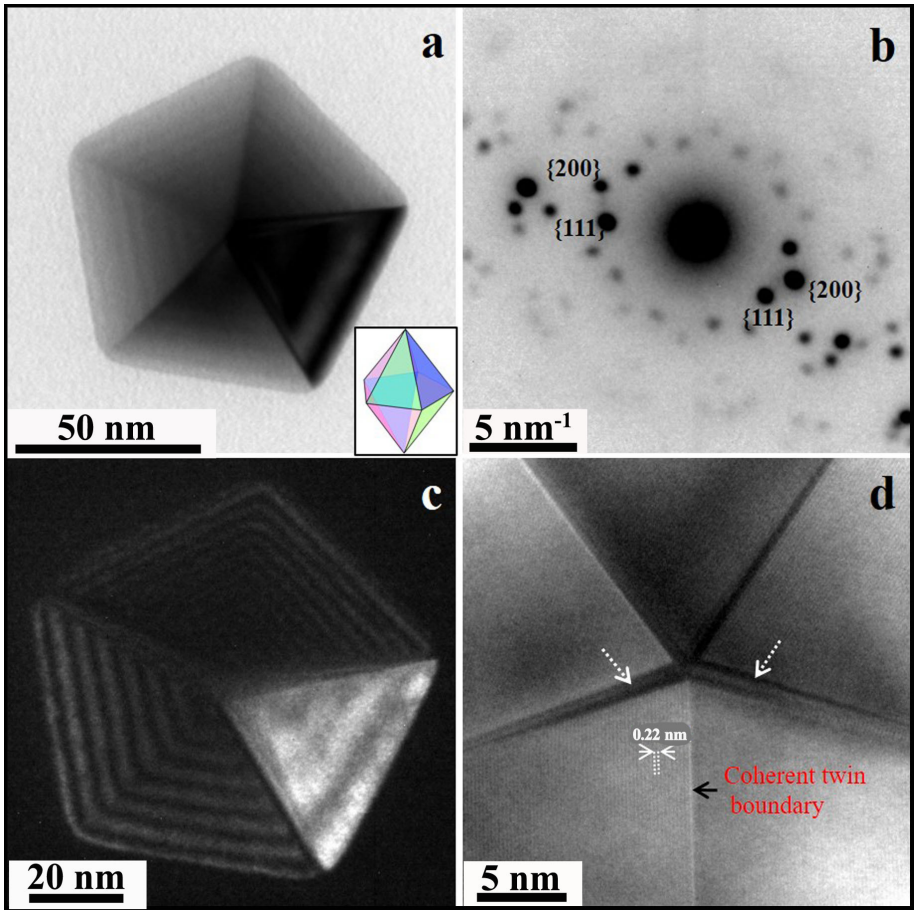

FIGURE 5.3: Bright field TEM image (a), SAD pattern along $< 110 >$ (b), dark field image (c) and HRTEM image of tip of the pentagon Au nanoparticles (d).

with those of pentagonal ones over 30 minutes periods may be due to limitation in control synthesis of seeds and determination of disappearance of charge transfer to solvent (CTTS) peak which is essentially a complete conversion of Au^{3+} to Au^{+} [202, 210]. This appears to be an essential condition to promote faceted growth of the seeds as ratio of Au^{+} to Au^{3+} determines the reaction kinetics and finally the population ratio of pentagons and triangular Au NPs. This understanding is helpful in tailor making of desired shape of the nanoparticles. Detailed structural and microstructural studies are done through bright field (BF), dark field (DF), selected area electron diffraction (SAD) and HRTEM of the individual nanoparticles (NPs). Figures 5.3 (a)- (d) depict BF, SAD, DF and HRTEM micrographs of the Au pentagon. From BF the average size of the edges of the Au pentagons are found to be $\sim$ 50 nm. Further, five twin boundaries with thickness fringes are clearly visible. The appearance of thickness fringes and their variable spacing from edge to center suggests that this shape is not a planar pentagon. Therefore, α-tilting of the sample within instrumental limit of TEM (± 45º) was performed and changes of shape from pentagon to rhombus and vice-versa was observed as shown in Figure 5.4.

This leads to the conclusion that pentagonal shapes are rather pentagonal bipyramids. These pentagonal bipyramids may be thought of a structure composed of tetrahedra, each of which is bounded by $\{111\}$ type planes. The presence of almost equal sized edges (regular pentagon) suggests that viewing direction is nearly parallel to $< 110 >$. Therefore, it is expected that all $\{111\}$ facets should equally diffract. But from the observed BF image one sector is found to be strongly diffracting which suggests that this $\{111\}$

plane is oriented differently from regular 3-fold cubic $\{111\}$ planes. This may be understood by recalling that if icosahedron is viewed along any one of the 2-fold axes then a set of four of the fifteen 3-folds possesses cubic orientation. When this is seen along any 5-fold direction then one encounters two consecutive non cubic 3-folds and two cubic 3-folds separated by a non-cubic 3-fold. As a consequence of this, one notices two types of distinct contrast in the five triangular sectors (cf. Figure 5.3 (a)). This has clearly been brought out in Figure 5.5.

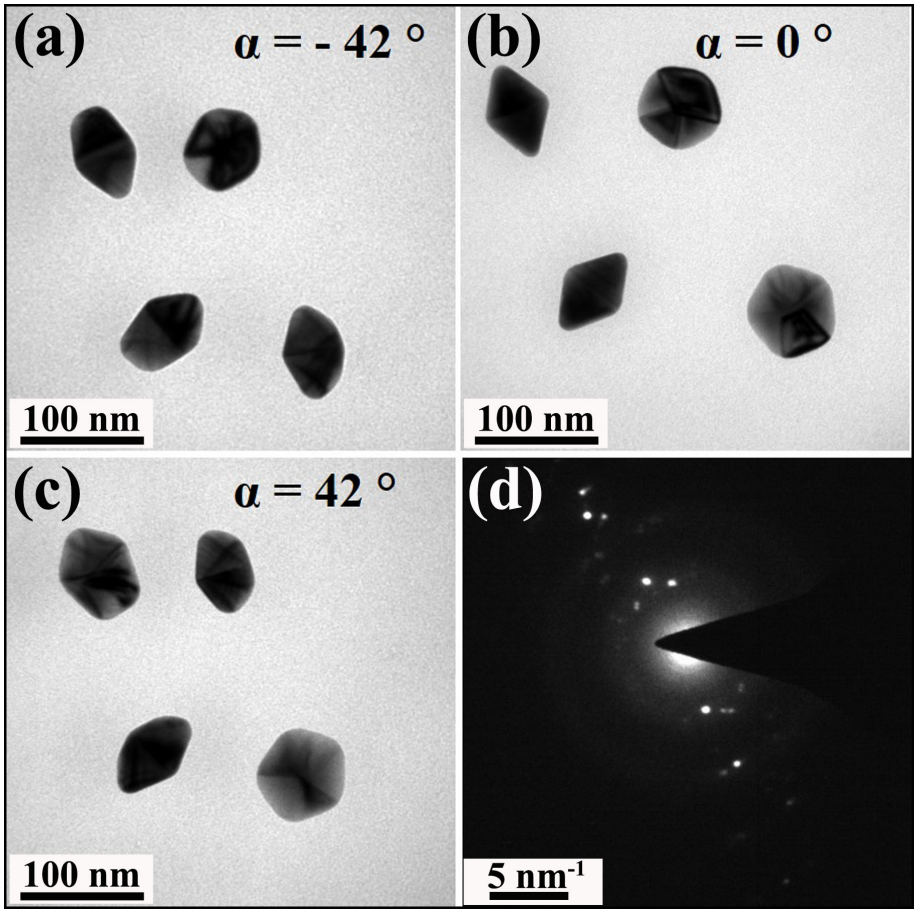

FIGURE 5.4: Systematic α-tilt study of Au nanoparticles.

However, the pentagonal bipyramid particles do not have all the essential geometrical features of icosahedra. Selected area diffraction pattern captured from the pentagon (shown in BF image) is displayed in Figure 5.3 (b). The DP is indexed to two $\{200\}$ types and four $\{111\}$ types reflections. This corresponds to the strongly diffracting pair of $\{111\}$ planes as seen in the BF image. Splitting of the $\{111\}$ planes as observed in the DP is due to presence of rotational twins [219, 220]. When sample was slightly tilted all the ten sets of $\{200\}$ and $\{111\}$ reflections corresponding to all the five sectors can be noticed as shown in Figure 5.3 (b). Dark field image (Figure 5.3 (c)) also shows the similar thickness fringes as observed in BF image conforming to the shape of pentagonal bipyramid.

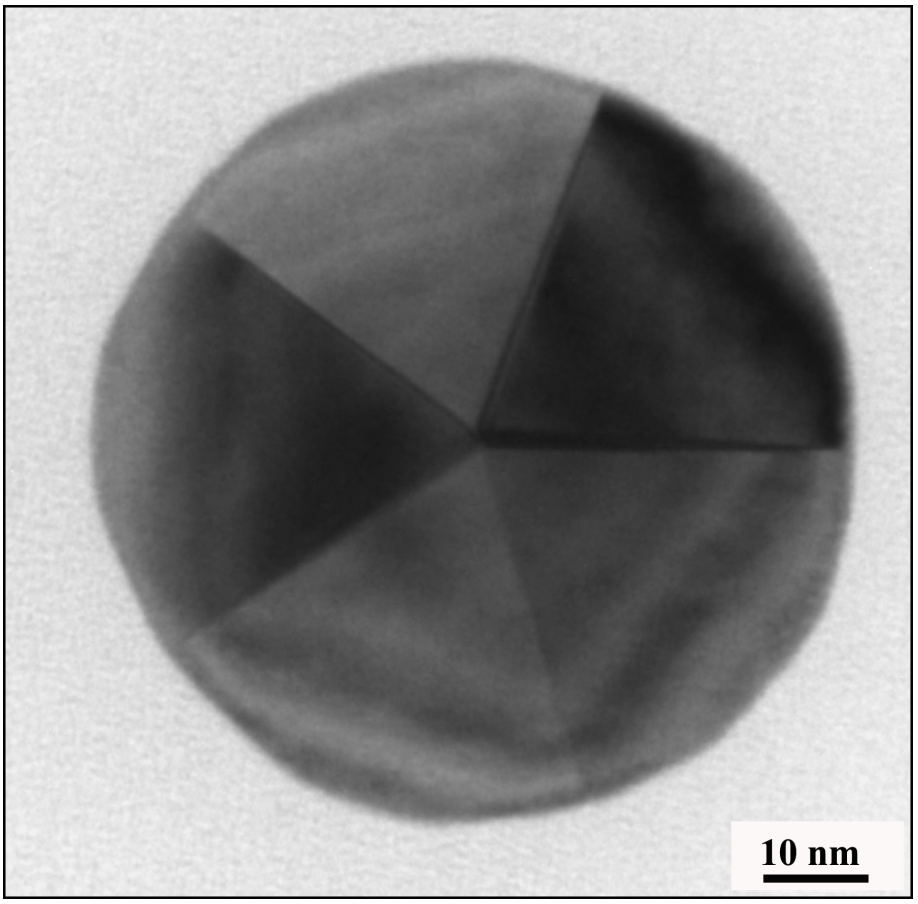

FIGURE 5.5: Bright field TEM micrograph of pseudospherical Au nanoparticles.

Such a shape is also described as decahedral particle in literature [202]. However, instead of five triangular sectors two rhombus like and a triangular sector are observed when dark field was captured from the pair of two $\{111\}$ and a $\{220\}$ reflections.The high resolution TEM micrograph from the apex of pentagonal bipyramid oriented close to $< 110 >$ zone is shown in Figure 5.3 (d). Five sharp twin boundaries are noticed which implies that pentatwinned structures is a result of growth with its history lying in the seed particle rather than physical attachment of 10 tetrahedra. The statement made while discussing Figure 5.3 with respect to two different types of 3-folds is further qualified by the boundaries between the rotational variants. One of the boundaries seems to suggest coherency between the two twins (marked as arrows in Figure 5.3 (d)) whereas other two orientations are thick (marked by dotted arrow). Interestingly, average d-values ($\sim$ 2.25 Å) measured from lattice fringes from all the sectors differs from that of standard Au $\{111\}$ inter-planar spacing (2.355 Å) (PDF card no. 00-004-0784). This point will be discussed again after presenting TEM results from triangular particle. BF image of a triangular particle is shown in Figure 5.6 (a). The triangular particle in its interior appears uniformly dark owing to proper orientation along $\{111\}$ plane. Length of the edges is measured to be $\sim$ 100 nm. Interestingly, thickness fringes are observed only along edges which indicate that this triangular particle is indeed truncated tetrahedron. The SAD pattern of the truncated tetrahedron shown in Figure 5.6 (a) is depicted in Figure 5.6 (b). All the spots in the DP was indexed to $\{220\}$ and $\{224\}$ reflections corresponding to $< 111 >$ zone axis. Each of the $\{220\}$ reflections were found to contain six streaked spots arranged in two inverted

triangles around them. All the Braggs spots in this zone display such a feature after tilting by $\sim$ 1- 2^o in the double tilt holder. They clearly indicate arising due to shape of the particle at such length scale as mentioned in literature [215]. Dark field was captured from $\{220\}$ and $\{224\}$ reflections as shown in Figure 5.6 (c). In both cases base of the truncated tetrahedron appears dark as it is $\{111\}$ plane which is not expected to appear in $< 111 >$ zone. However, thick band along the edges (region of thickness fringes in BF image) were observed bright in DF from $\{220\}$ reflection. On the contrary, only sharp edges were illuminated in DF from $\{224\}$. This observation conforms to aforesaid assertion related to the shape to be truncated tetrahedron. Owing to thickness limitation lattice fringes at high magnification could not be resolved. Therefore, sample was tilted along one of the edge of truncated tetrahedron and $\{111\}$ planes was resolved with spacing $\sim$ 2.29 Å which is smaller than that of standard $\{111\}$ d-values as noted earlier. Tilting the sample alters the shape corresponds to projection of tilted truncated tetrahedron as shown in Figure 5.6 (d). In addition to two inverted triangles around the Braggs reflections in this zone, one more interesting feature appears. This refers to appearance of forbidden spots at 1/3$\{422\}$ and 2/3$\{422\}$.

It has been argued in the literature that 1/3$\{422\}$ forbidden reflections in Ag and Au nanoprisms may arise for varieties of reasons [203, 214, 215, 221]. The common thread for all of them refers to stacking faults that are introduced during the growth process. Out of the six models enumerated in Appendix II of the paper [214], one of them is applicable in this work. This relates to the creation of monoatomic surface steps on the $\{111\}$ growing face leading to breaking of regular FCC interference pattern. This, in

turn, gives rise to 1/3{422} reflections (cf. Fig. 5.7 d). The stacking fault that causes breaking of regular stacking sequence of .... ABCABCABC.... must be intrinsic in nature in this case. The removal of any layer (say layer A indicated by V) may give rise to ....ABCVBCABC.... . Such a removal of layer apart from giving rise to 1/3{422} reflections leads to decrease in average lattice parameter of FCC cell in the truncated tetrahedral particle. The density of occurrence of intrinsic faults may vary from one truncated tetrahedral particle to others. This is the most likely reason that a variation of lattice parameters has been noted. The variation in intensities of these forbidden reflections is

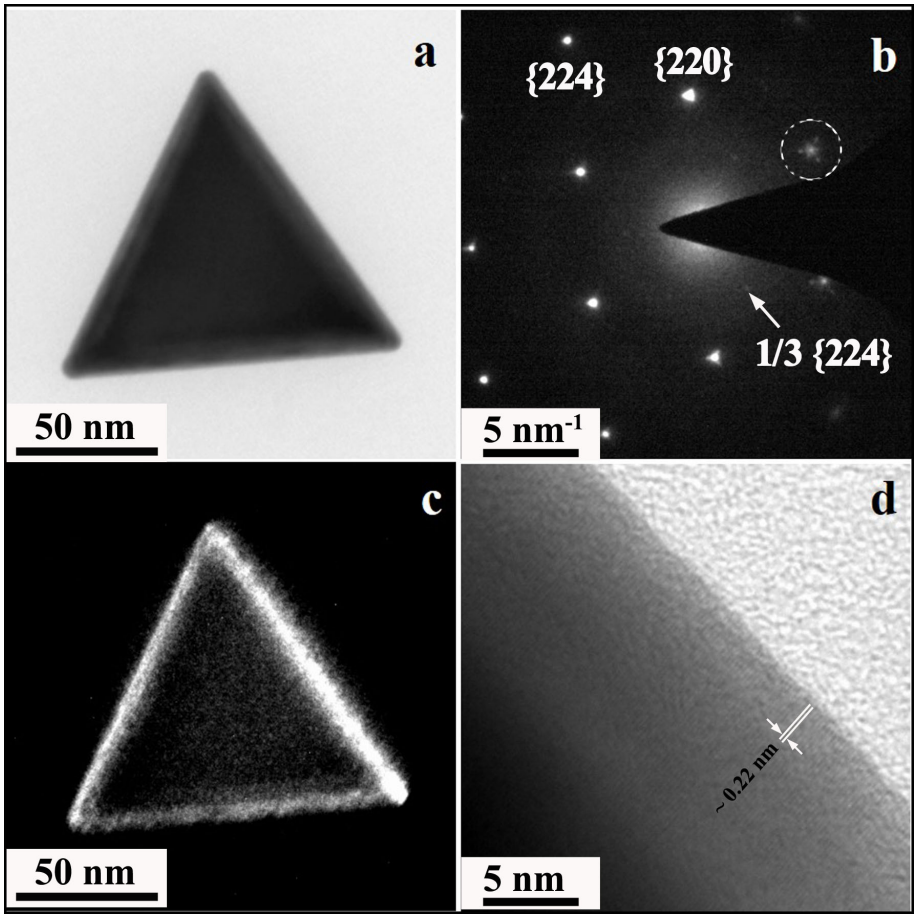

FIGURE 5.6: Bright field TEM image (a), SAD pattern along $< 111 >$ (b), dark field image (c) and HRTEM image of tilted trigonal Au nanoparticles (d).

dependent on density of intrinsic faults and associated dynamical effects. Both these reflections refer to allowed reflections for HCP stacking sequence [215]. It should be noted that extremely fine nano-domains of HCP will be present in the particle. The presence of such an intrinsic fault can be corroborated by referring to BF image shown in Figure 5.7 (a). Similar features are noticed at the slanted surface of the truncated tetrahedral particles Figure 5.7 (c). It is important to note here that these are extremely fine $\sim$ 3.0 nm lamellar of HCP and it has not been possible to resolve them under HRTEM. One may notice

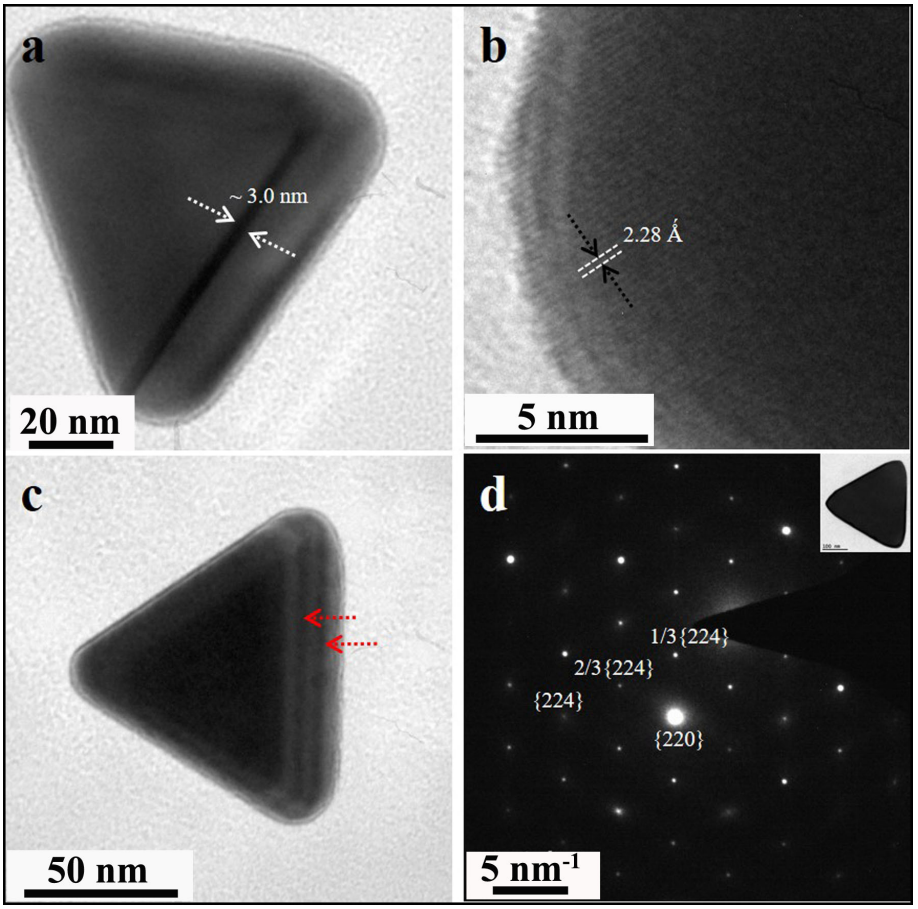

FIGURE 5.7: Bright field TEM image of truncated tetrahedral Au NPs showing a thin dark region of 3.0 nm indicating fault (a), HRTEM micrograph depicting edge of the particle after tilting 2-3 degree (b), BF micrograph with surface steps (shown by arrows) (c) and SAD pattern of another truncated tetrahedral Au NPs showing forbidden spots (d).

strong diffracting contrast in the central region of the particle. As a consequence, lattice fringes could be seen only at the edge of the particle as shown in Figure 5.7 (b). The spacing is closer to those of $\{111\}$ interplanar spacing of a FCC cell with lattice parameter of $\sim$ 3.95 Å from 4.078 Å.

5.3.2 LSPR behavior of faceted Au nanoparticles

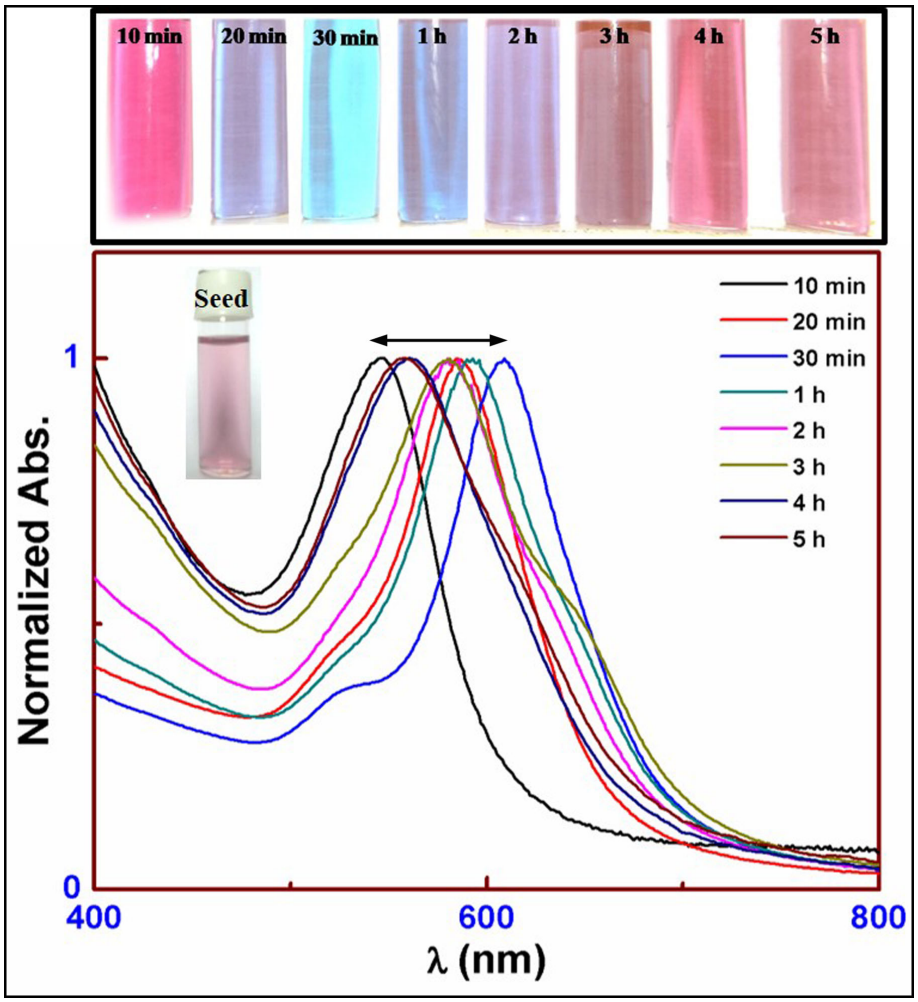

FIGURE 5.8: Observed color variation of sols including the seed. The UV-Vis spectra of samples grown from 10 min to 5 h are also shown.

The UV-Vis absorbance spectra were recorded to study the localized surface plasmon resonance (LSPR) behavior of the faceted Au nanocrystals. These are presented in Figure 5.8. The absorbance maximum (λ_{max}) of the seed was observed at $\sim$ 525 nm. The λ_{max} corresponding to 10 min, 20 min, 30 min, and 1 h were found to be at $\sim$ 545 nm, 585 nm, 609 nm, and 591 nm respectively. Apart from seed and 10 minutes grown sample all other samples show a shoulder $\sim$ 525 nm. This can be attributed to the anisotropy induced splitting of LSPR peak [116] . At 10 minutes shape evolved was not prominent but increased average particle size leads to a red shift in the plasmon band [222]. The samples grown at 20 minutes onwards faceted nanoparticles are clearly observed which gives rise to splitting in the LSPR peak. As the growth proceed particles with sharper facets leads to the further red shift in plasmon peak as evidenced in 30-minute sample. LSPR profile of 30 minutes grown sample shows main plasmon peak $\sim$ 591 nm and a prominent shoulder at $\sim$ 640 nm. Such plasmonic effects at 30 min and thereafter are due to interplay of the triangular and pentagonal faceted particles. One therefore, does not observe any significant change in the nature of UV-Visible absorbance spectra.

5.4 Conclusions

Growth of various morphologies through seed based synthesis of nanoparticles has been demonstrated. Morphologies of these nanoparticles primarily relate to decahedral and truncated tetrahedral shapes. Their relative abundance is dependent on temporal evolution of nanoparticles. Seed based synthesis gives us parameter to tailor-make shapes of

desired morphologies. The only requirement for such an accomplishment refers to possession of point group by the seed that serves as a supergroup of all the resulting particles. The usual pentagonal twinned morphologies having two distinct types of interfaces arise due to cubic and icosahedral three-fold orientations. Such a discussion is lacking in literature. One of the interesting diffraction features from the truncated tetrahedral particles refer to triangular streaks around Bragg spots conforming to underlying three-fold symmetry possessed by them. Another relate to existence of forbidden reflections of the types 1/3$\{422\}$ and 2/3$\{422\}$ along $< 422 >$ with allowed FCC reflections. Former has been interpreted in terms of particle shape effect whereas latter has been understood in terms of intrinsic fault. The variation of intensities for these forbidden reflections seems to be arising out of presence of nano-domains and their density. Invoking intrinsic fault for delineating aforesaid issues also helped us rationalize decrease of lattice parameter vis-à-vis that of standard FCC gold.